Self-similar solutions for the diffraction of weak shocks

Allen M. Tesdall * John K. Hunter †

Abstract. We numerically solve a problem for the unsteady transonic small disturbance equations that describes the diffraction of a weak shock into an expansion wave. In the context of a shock moving into a semi-infinite wall, this problem describes the interaction between the reflected part of the shock and the part that is transmitted beyond the wall. We formulate the equations in self-similar variables, and obtain numerical solutions using high resolution finite difference schemes. Our solutions appear to show that the shock dies out at the sonic line, rather than forms at an interior point of the supersonic region.

AMS subject classification. Primary: 65M06, 76H05; Secondary: 35M30, 35L65.

May 26, 2012

1 Introduction

In classical numerical simulations of steady transonic flow over an airfoil, the shock which terminates the supersonic region appears to form exactly on the sonic line (see, for example, [1, 3, 5, 6, 7]). However, high-resolution numerical calculations done on this problem and a corresponding situation in pseudo-steady two-dimensional flow in [8] show that the shock actually forms at a point where the underlying system (steady or self-similar) is strictly hyperbolic, and the flow is supersonic. The calculations in [8] show that the shock forms when compressive characteristics reflect off the sonic line and converge inside the supersonic, hyperbolic region. This mechanism of shock formation had originally been proposed by Guderley in [2].

The numerical experiments in [8] provide a direct observation of Guderley's proposed supersonic shock formation. Those experiments suggest that shock formation generically occurs inside the supersonic region and away from the sonic line, although it may be possible in specific situations to cause the characteristics to converge exactly on the sonic line.

In this paper we numerically study a problem related to the formation of a shock described above: it is the *disappearance* of a shock that diffracts self-similarly into an expansion wave. We express the governing equations in self-similar variables, and we

*Department of Mathematics, College of Staten Island, City University of New York, Staten Island, NY 10314 (allen.tesdall@csi.cuny.edu). Research supported by Department of Energy grant DE-SC0001378 and Research Foundation of CUNY grant 60145-39 40.

†Department of Mathematics, University of California at Davis, Davis, CA 95616 (jkhunter@ucdavis.edu). Research partially supported by National Science Foundation grant DMS-1009538.

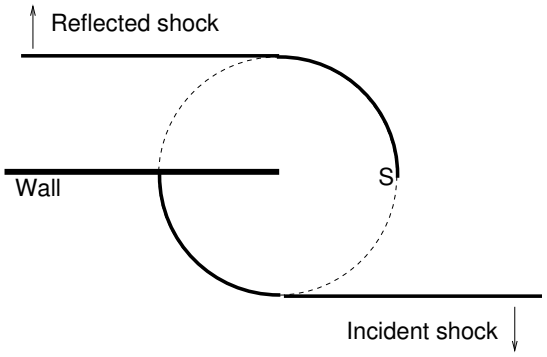

Figure 1.1: A weak shock moving downwards at slightly supersonic velocity, into and past a semi-infinite wall. Solid lines are shocks; dotted lines are expansion waves.

solve the self-similar equations using high-resolution schemes. We obtain solutions that are highly refined in the area of the shock disappearance point. In view of the numerical solutions for shock formation in [8], our solutions for shock disappearance are perhaps surprising: they appear to show that the shock disappears exactly on the sonic line, and not at a supersonic point.

We now describe the physical basis for the shock diffraction problem we solve here, which was introduced in [4]. Consider a weak plane shock moving at Mach number M slightly larger than 1 into a semi-infinite wall, as in Fig. 1.1. This problem is self-similar, so the solution depends only on $(x/t, y/t)$, where x and y are spatial coordinates and t is time. The incident shock diffracts around the wall, and an expansion wave (dotted line) propagates behind it. The reflected shock also diffracts around the wall, meeting the diffracted expansion at the point S. At S, there is a continuous transition from shock wavefront to expansion wavefront, and one of the main questions concerning this transition point is whether or not it is sonic. It is the solution near S that we seek.

An asymptotic matching analysis, described in [4], shows that the solution near a point such as S is given in the weak shock limit by the solution of an "inner" shock-diffraction problem for the unsteady transonic small disturbance equations (UTSDE). This inner problem consists of the UTSDE together with matching data, and is given in Section 2 (equations (2.1)–(2.2)). In this paper, we present numerical solutions of this inner shock-diffraction problem for the UTSDE computed in self-similar coordinates. There are several advantages to using our self-similar formulation rather than the standard unsteady formulation of the equations. First, solving the problem in self-similar form enables local grid refinement procedures to be implemented relatively easily, because solutions of the self-similar equations are stationary. As well, a grid continuation procedure is possible, whereby solutions are partially converged on coarse grids, interpolated onto more refined grids, and ultimately fully converged on the most refined grid. Finally, numerical evidence ([9]) suggests that shocks are captured more sharply in numerical solutions of the self-similar equations than in solutions of the unsteady equations. We use extreme local grid refinement in order to determine the nature of the flow (sonic or supersonic) at the shock disappearance point S. Our motivation for solving a problem for the UTSDE valid only near the shock disappearance point, rather

than solving a problem for the full Euler equations on the global domain indicated in Fig 1.1, is that, for the same computational cost, we can obtain a much more finely resolved solution near the area of interest - the shock disappearance point - than we could using the Euler equations.

Preliminary numerical solutions of the shock-diffraction problem for the UTSDE were given in [4], and appeared to indicate that the shock disappears on the sonic line. The highly refined solutions presented in this paper provide further evidence that the shock disappearance point is exactly sonic (see Fig. 4.3, for example). In addition, we give here a detailed description of the numerical method, including a discussion of its stability. In this paper, we also describe the effect of using different (linearized and "nonlinearized") far field numerical boundary conditions, and we compare and contrast our numerical solutions for the self-similar diffraction of a shock into an expansion wave with solutions for shock formation in steady and pseudo-steady transonic flows.

The organization of the rest of the paper is as follows. In Section 2, we describe the shock-diffraction problem for the UTSDE, and in Section 3 we outline the numerical method used to solve this problem. In Section 4 we present our numerical solutions, which provide evidence that the shock disappearance point is a sonic point. In Section 5, we discuss questions raised by these solutions, and compare them to the numerical solutions for the formation of shocks in [8]. In Section 6 we summarize our conclusions.

2 The shock-diffraction problem for the UTSDE

The shock-diffraction problem for the UTSDE consists of the UTSDE,

$$\begin{aligned} &u_t + \left(\frac{1}{2}u^2\right)_x + v_y = 0, \\ &u_y - v_x = 0, \end{aligned} \tag{2.1}$$

in $t > 0$, with the initial, or matching, condition

$$\begin{aligned} &u \sim \alpha \frac{y}{t}\sqrt{-\left(\frac{x}{t} + \frac{y^2}{4t^2}\right)} \qquad \text{as } \frac{x}{t} + \frac{y^2}{4t^2} \to -\infty, \\ &u = 0 \qquad \text{for } \frac{x}{t} + \frac{y^2}{4t^2} \text{ sufficiently large and positive.} \end{aligned} \tag{2.2}$$

Here, the variables $u(x, y)$ and $v(x, y)$ are proportional to the x and y velocity components, respectively. The small positive parameter α is proportional to the strength of the wave. Solutions of (2.1)–(2.2) asymptotically describe, in the weak shock limit, solutions of the full Euler equations near a point where a shock propagates into a constant state and diffracts into an expansion wave. See [4] for details of the formulation of this problem.

The problem (2.1)–(2.2) is self-similar, so its solution depends only on $\xi = x/t$ and $\eta = y/t$. Writing (2.1) in terms of ξ and η we get

$$\begin{aligned} -\xi u_\xi - \eta u_\eta + \left(\frac{1}{2}u^2\right)_\xi + v_\eta = 0, \\ u_\eta - v_\xi = 0. \end{aligned} \tag{2.3}$$

The initial condition (2.2) in the unsteady problem (2.1)–(2.2) becomes a far field boundary condition in the corresponding self-similar formulation of the problem. Writing (2.2) in terms of ξ and η gives

$$u \sim \alpha\eta\sqrt{-(\xi + \frac{\eta^2}{4})}, \quad v \sim -\frac{2}{3}\alpha(-(\xi + \frac{\eta^2}{4}))^{3/2} \quad \text{as } \xi + \eta^2/4 \to -\infty. \tag{2.4}$$

The far field behavior of v given in (2.4) follows from the far field behavior of u and the second equation in (2.3). We also have from (2.2) that

$$u = 0, \quad v = 0 \qquad \text{for } \xi + \eta^2/4 \text{ sufficiently large and positive.} \tag{2.5}$$

Equations (2.3)–(2.5) are a formulation of the shock-diffraction problem in self-similar form. The data in boundary condition (2.4) exactly satisfies the linearization of (2.3). However, this data is continuous and has a square-root singularity at the wavefront, which in the linearized approximation is located at $\xi + \eta^2/4 = 0$. This is qualitatively incorrect since, at the wavefront, the solution of the nonlinear problem has a discontinuity across a shock and a finite jump in its derivative across an expansion. The following "nonlinearized" far field boundary data, which has the correct qualitative behavior at the wavefront (located in the nonlinearized approximation at $\xi + \eta^2/4 = 0$ for $\eta < 0$ and $\xi + \eta^2/4 = 3\alpha^2\eta^2/4$ for $\eta > 0$), was obtained in [4]:

$$\begin{aligned} u &\sim \alpha\eta\sqrt{-(\xi + \frac{\eta^2}{4}) + \alpha^2\eta^2} + \alpha^2\eta^2, \\ v &\sim -\frac{2}{3}\alpha\left(\sqrt{-(\xi + \frac{\eta^2}{4}) + \alpha^2\eta^2} + \alpha\eta\right)^3. \end{aligned} \tag{2.6}$$

Equations (2.6) provide more accurate far field matching data than the linearized matching data (2.4). We will refer to equations (2.3), (2.5)–(2.6) as the shock-diffraction problem in self-similar form.

Equation (2.3) is hyperbolic ('supersonic') when $u < \xi + \eta^2/4$, and elliptic ('subsonic') when $u > \xi + \eta^2/4$. It changes type across the sonic line

$$\xi + \frac{\eta^2}{4} = u(\xi, \eta). \tag{2.7}$$

For the numerical computations, it is convenient to define a "sonic function"

$$S = u - (\xi + \eta^2/4). \tag{2.8}$$

When $S < 0$ the flow is supersonic, and when $S > 0$ the flow is subsonic.

3 The Numerical Method

The numerical method we use was developed in [8, 9] specifically for solving self-similar problems for the UTSDE. The method uses special self-similar variables,

$$\begin{aligned} &r = \frac{x}{t} + \frac{y^2}{4t^2}, \qquad \theta = \frac{y}{t}, \qquad \tau = \log t, \\ &\widetilde{u} = u - r, \qquad \widetilde{v} = v - \frac{1}{2}\theta u. \end{aligned} \tag{3.1}$$

We note that the sonic line (2.7) is a parabola in the (ξ, η)-plane for a constant solution of (2.3) with, say, $u = u_0$ (for non-constant solutions the sonic line has some more complicated shape.) The coordinates in (3.1) have the effect of straightening the sonic line: for a constant state with $u = u_0$, (2.7) is a vertical line in the (r, θ)-plane with equation $r = u_0$. Writing (2.1) in terms of the variables in (3.1), and introducing a potential $\phi(r, \theta, \tau)$ such that

$$\widetilde{u}(r, \theta, \tau) = \phi_r, \quad \widetilde{v}(r, \theta, \tau) = \phi_\theta, \tag{3.2}$$

one gets

$$\phi_{r\tau} + \left(\frac{1}{2}\phi_r^2\right)_r + \phi_{\theta\theta} + \frac{3}{2}\phi_r + \frac{1}{2}r = 0. \tag{3.3}$$

Equation (3.3) forms the backbone of the numerical method. The advantage of the self-similar formulation (3.3) is that it can be solved using standard transonic finite difference techniques, in contrast to the situation for the usual self-similar formulation, given by (2.3). To illustrate this, the plots in Fig. 3.1(a) and (b) depict grid stencils indicating the mesh points used in a standard first-order upwind discretization of equations (2.3) and (3.3), respectively. (The discretization of (2.3) is with respect to ξ and η, while the spatial discretization of (3.3) is with respect to r and θ.) Both sets of stencils are plotted in the (ξ, η)-plane, and the parabolas in these plots are the sonic line (2.7) for a constant state. In these plots, upwind stencils are plotted at several sample mesh points in the supersonic portion of the flowfield. The characteristics of each family (which are tangent to the sonic line) are drawn through these sample points, labeled A, B, and C. In Fig. 3.1(a), at mesh point A the analytical domain of dependence, bounded by the two incoming characteristics, is contained in the numerical domain of dependence, bounded by the vertical segments, so the CFL condition is satisfied and the upwind discretization is stable. At mesh points like B and C, however, the analytical domain of dependence contains points outside of the numerical domain of dependence. Hence, the CFL condition is violated, and the standard upwind scheme for (2.3) is unstable (although it might be possible to design a stable scheme using some more complicated choice of stencil mesh points). On the other hand, in Fig. 3.1(b), because the grid is discretized with respect to the parabolic coordinate r, as indicated, the CFL condition is respected at all points in the supersonic portion of the flowfield. Hence, the upwind scheme for (3.3) is stable.

A crucial feature of the numerical method is the use of local grid refinement in the area of interest — here, the shock disappearance point. We build a sequence of successively refined, nonuniform, logically rectangular finite difference grids. Each grid uses uniform grid spacing inside a small box surrounding the shock disappearance point. Outside of this box, the grid is exponentially stretched in both grid directions. The uniform grid region of each grid in the sequence of grids is refined by a factor of two in relation to the uniform grid region of the preceding grid. We use grid continuation, in which solutions obtained on coarse grids are interpolated onto more refined grids and converged on those grids. We continue the refinement process until additional refinement results in no observable change in the solution near the shock disappearance point, indicating grid convergence. Details of our interpolation procedure, and further discussion of our grid continuation and grid refinement strategies, are given in [8].

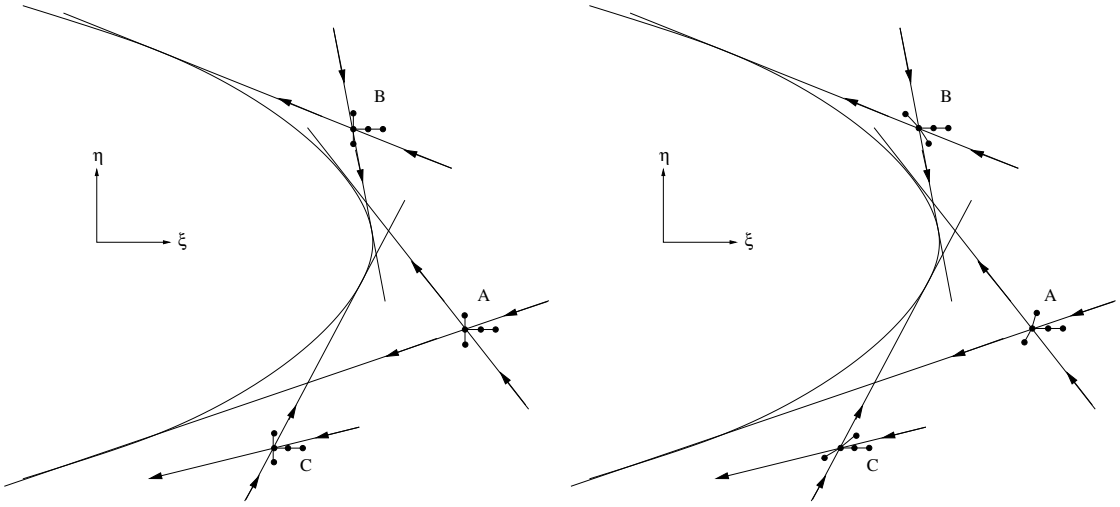

(a) Upwind scheme for (2.3) (unstable) **(b)** Upwind scheme for (3.3) (stable)

Figure 3.1: Stability of upwind differencing in the supersonic region. In (a), grid stencils for upwind discretization of the standard self-similar UTSDE (2.3), and in (b), stencils for upwind discretization of (3.3). The parabola in (a) and (b) is the sonic line (2.7) corresponding to a constant state. Flow to the right of the sonic line is supersonic, and flow to the left is subsonic.

The basic scheme for solving (3.3) is as follows. We define a non-uniform grid r_i in the r-direction and θ_j in the θ-direction, where $r_{i+1} = r_i + \Delta r_i^+$ and $\theta_{j+1} = \theta_j + \Delta\theta_j^+$. Denoting an approximate solution of (3.3) by $\phi_{i,j}^n \approx \phi(r_i, \theta_j, n\Delta\tau)$, where $\Delta\tau$ is a fixed time step, we discretize (3.3) in artificial time τ using

$$\frac{\phi_r^{n+1} - \phi_r^n}{\Delta\tau} + f(\phi_r)_r^n + \phi_{\theta\theta}^{n+1} + \frac{3}{2}\phi_r^{n+1} + \frac{1}{2}r = 0, \tag{3.4}$$

where the flux function f is defined by

$$f(\widetilde{u}) = \frac{1}{2}\widetilde{u}^2. \tag{3.5}$$

To make the notation simpler, we define discrete pseudo-velocities:

$$\widetilde{u}_{i,j} = \frac{\phi_{i+1,j} - \phi_{i,j}}{\Delta r_i^+}, \qquad \widetilde{v}_{i,j} = \frac{\phi_{i,j} - \phi_{i,j-1}}{\Delta\theta_j^-},$$

where

$$\begin{aligned} \Delta r_i^+ &= r_{i+1} - r_i, \\ \Delta\theta_j^\pm &= \pm(\theta_{j\pm1} - \theta_j). \end{aligned}$$

Then our discrete approximation to (3.3) is

$$\begin{aligned} \frac{\widetilde{u}_{i,j}^{n+1} - \widetilde{u}_{i,j}^n}{\Delta\tau} &+ \frac{F(\widetilde{u}_{i,j}^n, \widetilde{u}_{i+1,j}^n) - F(\widetilde{u}_{i-1,j}^n, \widetilde{u}_{i,j}^n)}{\Delta r_i^+} + \frac{\widetilde{v}_{i,j+1}^{n+1} - \widetilde{v}_{i,j}^{n+1}}{\frac{\Delta\theta_j^+ + \Delta\theta_j^-}{2}} \\ &+ \frac{3}{2}\widetilde{u}_{i,j}^{n+1} + \frac{1}{2}r_i = 0. \end{aligned} \tag{3.6}$$

In this equation, F is a numerical flux consistent with the flux f in (3.5). In our computations, we use a second-order minmod-limited numerical flux (see [9] for details).

In terms of the potential ϕ defined in (3.2), the boundary conditions (2.5)–(2.6) become (see [4])

$$\phi(r,\theta) = \begin{cases} \alpha^2 r\theta^2 - \frac{2}{3}\alpha^4\theta^4 - \frac{2}{3}\alpha\theta(-r+\alpha^2\theta^2)^{3/2} - \frac{1}{2}r^2, & \theta < 0, r \le 0, \\ -\frac{r^2}{2}, & \theta < 0, r > 0, \\ \alpha^2 r\theta^2 - \frac{2}{3}\alpha^4\theta^4 - \frac{2}{3}\alpha\theta(-r+\alpha^2\theta^2)^{3/2} - \frac{1}{2}r^2, & \theta \ge 0, r \le \frac{3\alpha^2\theta^2}{4}, \\ -\frac{r^2}{2}, & \theta \ge 0, r > \frac{3\alpha^2\theta^2}{4}. \end{cases} \tag{3.7}$$

In order to solve the shock-diffraction problem in self-similar form (equations (2.3), (2.5)–(2.6)), we solve equation (3.6) subject to boundary condition (3.7). Because the problem we are solving is self-similar, the time derivative term in (3.6) vanishes as $\tau \to +\infty$ (the same is true for (3.3), from which (3.6) was obtained by discretization.) Hence, we solve (3.6) by iterating a solution forward in artificial time τ until it converges to a steady state. We sweep from right to left in r, consistent with the direction of propagation of the characteristics for (2.3), which is in the $-r$ direction. Additional discussion of the numerical method is given in [8, 9].

4 Numerical Results

We computed solutions of (2.3), (2.5)–(2.6) for α equal to 0.2, 0.3, and 0.4. Figure 4.1 gives an overall picture of the solution for each of the three values of α. The plots on the left of Fig. 4.1 are contour plots of u as a function of $(x/t, y/t)$. The plots on the right present an alternate depiction of u as a function of $(x/t, y/t)$, with u plotted as a surface $z = u(x/t, y/t)$ instead of as contours. The dashed red line in the plots in (a), (c) and (e) is the sonic line (2.7). Flow to the right of the sonic line is supersonic, and flow to the left of it is subsonic. The u-contour levels are indicated on the contour plots. The computational domain has curved left and right boundaries because of the coordinates used in (3.1).

The plots in Fig. 4.1 show that there is a shock located at the sonic line for y/t greater than some given value (which is a function of α) that we will call $(y/t)_*$, and an expansion wave at the sonic line for $y/t < (y/t)_*$. At $y/t = (y/t)_*$, the shock appears to reach zero strength and turn continuously into an expansion wave. For example, for $\alpha = 0.3$, from the plots in (c) and (d) the shock appears to reach zero strength at a value of $(y/t)_*$ close to -2. For a fixed value of α the shock strength increases as y/t increases, as shown. Additionally, as α increases, the shock wavefront increases in strength, and moves further to the right (this is the reason that the right numerical boundary for $\alpha = 0.4$ was extended further to the right than it was for the lower values of α, as shown in Fig. 4.1(e)).

In order to determine more accurately where the shock reaches zero strength, in Fig. 4.2(a) we plot u-contours and the sonic line in a small region near the apparent shock disappearance location, for $\alpha = 0.3$. In this region local grid refinement was used. The locally refined grid size and the u-contour spacing are given in the figure caption. Because the state ahead of the sonic line is constant with $u = 0$, and u jumps from this value ahead of the shock to positive values behind it, the point where the shock

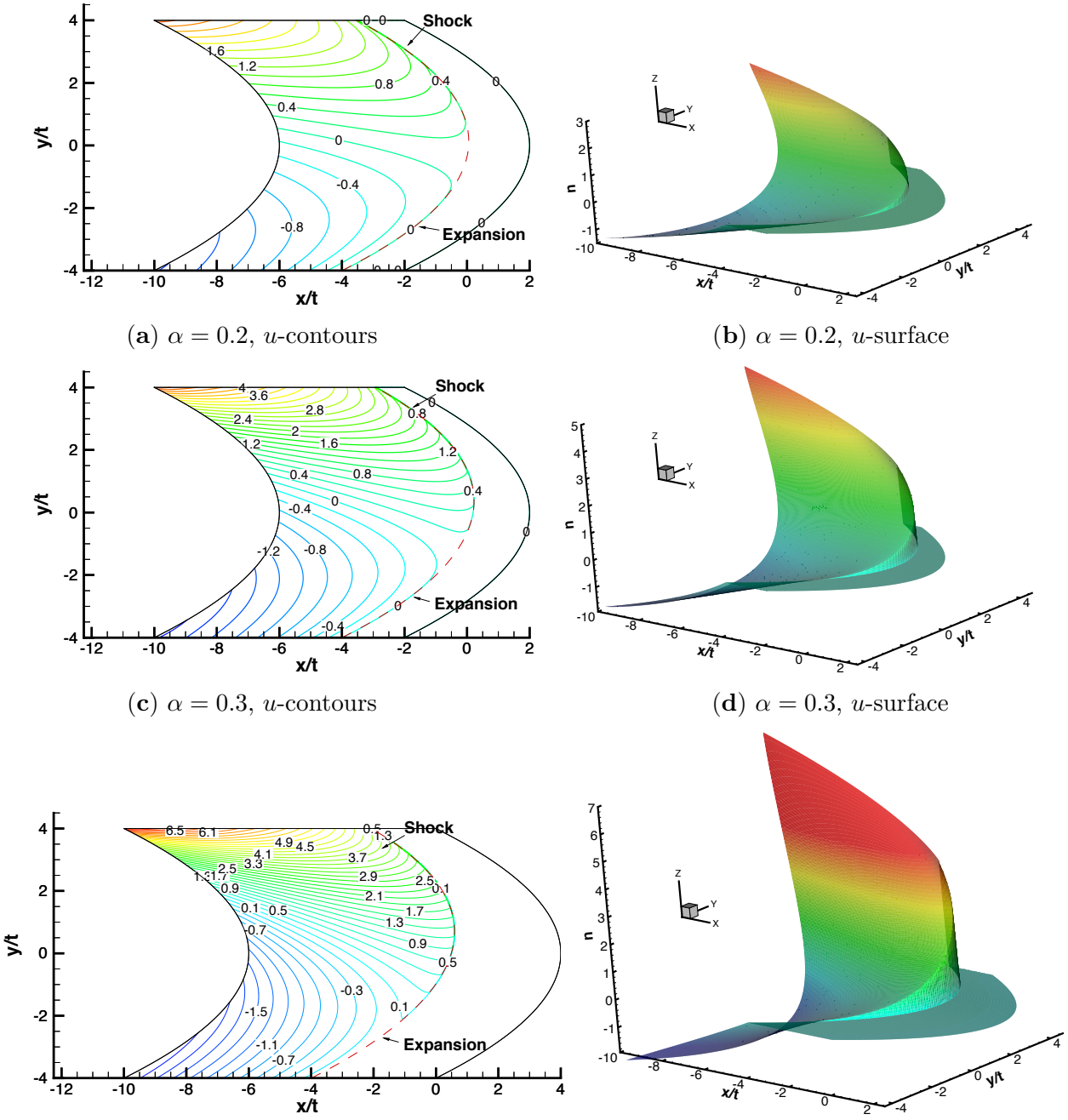

(**a**) $\alpha = 0.2$, u-contours

(**b**) $\alpha = 0.2$, u-surface

(**c**) $\alpha = 0.3$, u-contours

(**d**) $\alpha = 0.3$, u-surface

(**e**) $\alpha = 0.4$, u-contours

(**f**) $\alpha = 0.4$, u-surface

FIGURE 4.1: Contour plots ((a), (c), and (e)) and surface plots ((b), (d), and (f)) of u for increasing values of α. The dashed red line in (a), (c), and (e) is the sonic line. The nearly vertical jump in the surface plots on the right is the shock.

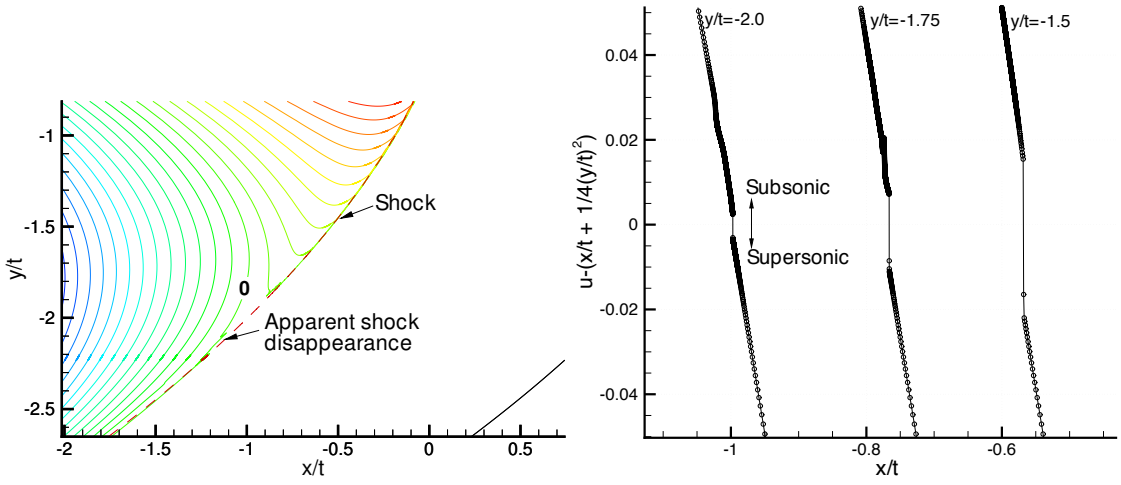

(a) **(b)**

Figure 4.2: In (a), a contour plot of u close to the shock die out point, $\alpha = 0.3$. The flow is supersonic to the right of the sonic (dashed) line, and subsonic to the left; the $u = 0$ contour is indicated on the plot. The u-contour spacing is 0.015. The region shown contains the refined uniform grid, which has 3000×3000 grid points ($\Delta(x/t) = \Delta(y/t) = 1 \times 10^{-5}$). In (b), cross sections of the sonic function S taken through the shock at $y/t = -1.5$, $y/t = -1.75$, and $y/t = -2$. The high-resolution numerical method captures the shock in one to two points, as shown.

disappears is located approximately at the intersection of the $u = 0$ contour with the sonic line. This contour is indicated on the plot, and, from the plot, the point where the shock dies out appears to be located at $(y/t)_* \approx -2.2$. In Fig. 4.2(b) we plot cross sections of the sonic function S (equation (2.8)) taken horizontally through the shock at three values of y/t slightly above this shock disappearance point. As the shock is crossed from right to left in the direction of flow, S jumps from negative (supersonic) values to positive (subsonic) values, as shown, so the shock is a transonic shock at these locations. The shock strength, as measured by the jump in S, is quite weak at $y/t = -2.0$, as indicated. However, these cross sections do not show what happens very close to the point where the shock disappears, which occurs at a lower value of y/t than those shown here.

The plots in Figs. 4.1–4.2 appear to show that the shock dies out at a point on the sonic line, rather than inside the supersonic region. In order to determine whether the shock dies out exactly on the sonic line, in Fig. 4.3 we plot cross sections of the sonic function S taken horizontally across the shock at four closely spaced values of y/t very close to the apparent shock disappearance location $(y/t)_* \approx -2.2$. Proceeding in the direction of decreasing y/t, the shock profiles at $y/t = -2.2, -2.225$, and -2.25 resemble those in Fig. 4.2(b), and indicate that the shock is transonic (and very weak) at these locations. At $y/t = -2.275$, as shown, the shock has almost completely disappeared. (For smaller values of y/t, the jump in S completely disappeared, being replaced by a continuous transition which remained centered on $S = 0$.) Because the

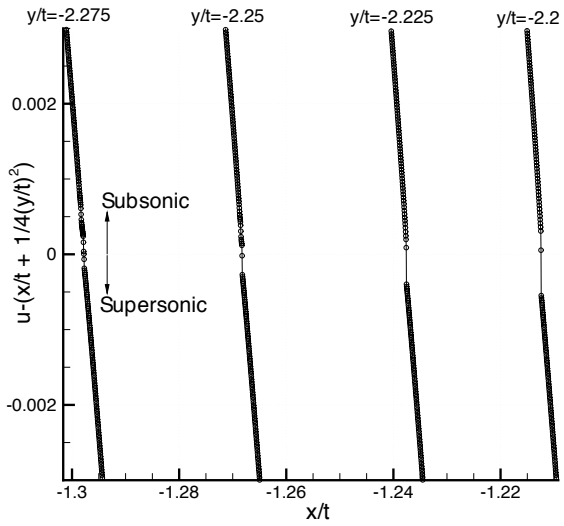

Figure 4.3: Cross sections of the sonic function S taken horizontally across the shock very close to the apparent disappearance point. The shock appears to die out at $y/t \approx -2.275$, on the sonic line.

jump in S at $y/t = 2.275$ is from a supersonic to a subsonic value, the shock dies out on the sonic line, at approximately this location.

In order to illustrate the behavior of the solution of the shock-diffraction problem as $\alpha \to 0$, in Fig. 4.4 we plot u-contours and the sonic line for a sequence of solutions with α equal to 0.1, 0.05, and 0.01. The contour lines are plotted at the same levels of u in these plots; however, as α decreases there is less variation in the solution, so that fewer contour lines appear. In all of these solutions, the shock appears to die out on the sonic line (the disappearance point being indicated by the intersection of the sonic line with the $u = 0$ contour), consistent with the result presented above for $\alpha = 0.3$. These solutions also show that the distance the shock diffracts into the half-plane $y/t < 0$ approaches zero as the shock strength, measured by α, approaches zero. When $\alpha = 0$, the shock disappears entirely and there is smooth undisturbed flow.

Finally, it was pointed out in Section 2 that the "nonlinearized" matching data (2.6), which we used in our computations, provides more accurate far-field matching data than the linearized data (2.4). In Figure 4.5, we illustrate the effect on the solution of the use of this nonlinearized matching data. Figure 4.5(a) shows u-contours from a computation using (2.4) as the numerical boundary condition, with $\alpha = 0.3$. For comparison, the solution computed using (2.6) as the boundary condition is shown in the plot in 4.5(b) (this solution was depicted earlier in Fig. 4.1(c)). These solutions were computed using identical grids, and the contour levels are shown on the plots. The solutions are qualitatively similar, but the values of u at identical locations $(x/t, y/t)$ are different. The shocks in the two solutions are also in different locations. Additionally, the sonic (dashed) line in the solution computed using the linearized data does not exit the numerical domain smoothly, but reflects off the bottom boundary. This appears to be caused by a mismatch between the actual solution and the solution enforced at the boundary by the condition (2.4).

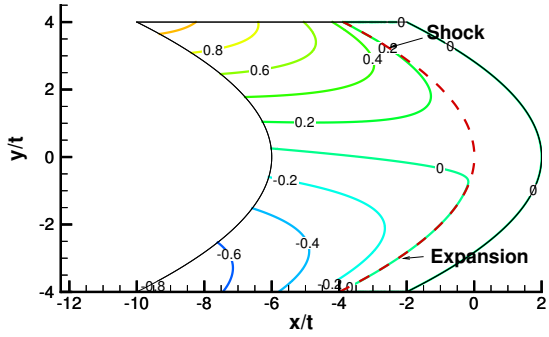

(**a**) $\alpha = 0.1$

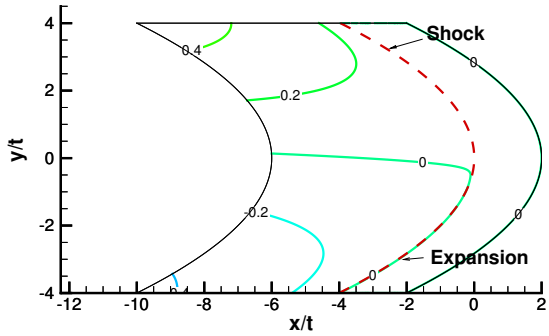

(**b**) $\alpha = 0.05$

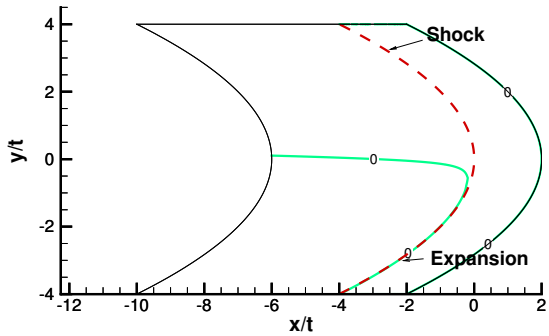

(**c**) $\alpha = 0.01$

Figure 4.4: A sequence of u-contour plots showing the behavior of solutions as the small parameter α approaches zero. The u-contour spacing in (a), (b), and (c) is 0.2. The dashed red line in these plots is the sonic line. When $\alpha = 0.01$, (see (c)), the flow field is nearly uniform.

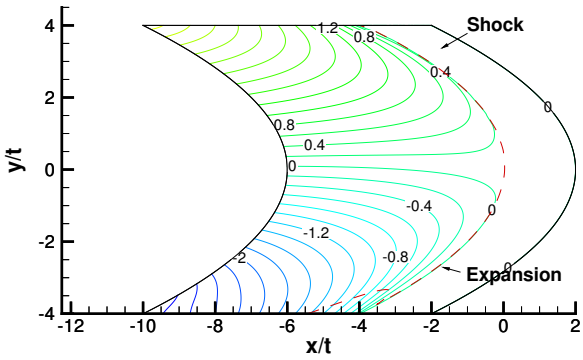

(a) Linearized BC (equation (2.4))

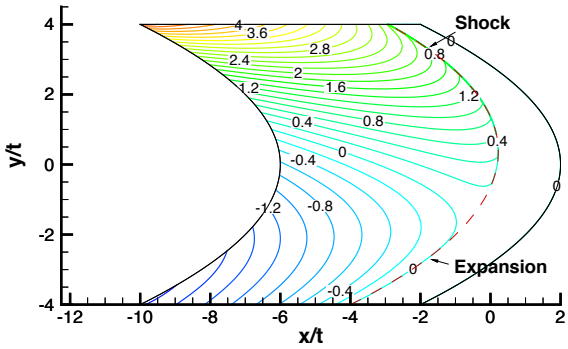

(b) Nonlinearized BC (equation (2.6))

Figure 4.5: Contour plots of u showing the effect of use of (a) linearized, and (b) nonlinearized matching data. The contour spacing is 0.2 in both (a) and (b), and both solutions were computed using a uniform grid with 1000×1000 points. The dashed red line is the sonic line.

5 Discussion

These numerical results, showing the disappearance of a shock on a sonic line, contrast with the numerical solutions of steady and self-similar transonic flow problems in [8], which show the formation of shocks away from the sonic line. We illustrate this contrasting behavior in Fig. 5.1. The plot in Fig. 5.1(a) shows a numerical solution of the steady transonic airfoil problem for the steady TSDE, as obtained in [8]. The plot shows u-contours and the sonic line in a region containing the supersonic bubble and terminal shock over the airfoil, and illustrates that the shock appears to form on or very close to the sonic line. The plot in (b) shows cross sections of a sonic function for the steady TSDE taken across the shock near the apparent formation point (as indicated, negative values of this sonic function indicate supersonic flow and positive values indicate subsonic flow). The y locations at which the cross sections were taken are indicated on the plot in (b). These cross sections indicate that the shock forms at $y \approx 0.230$. Further, cross sections taken very close to this value of y contain jumps in sonic function from supersonic to supersonic values, as shown, which indicates that the shock forms in the supersonic region. Similarly, the plot in Fig. 5.1(c) depicts a

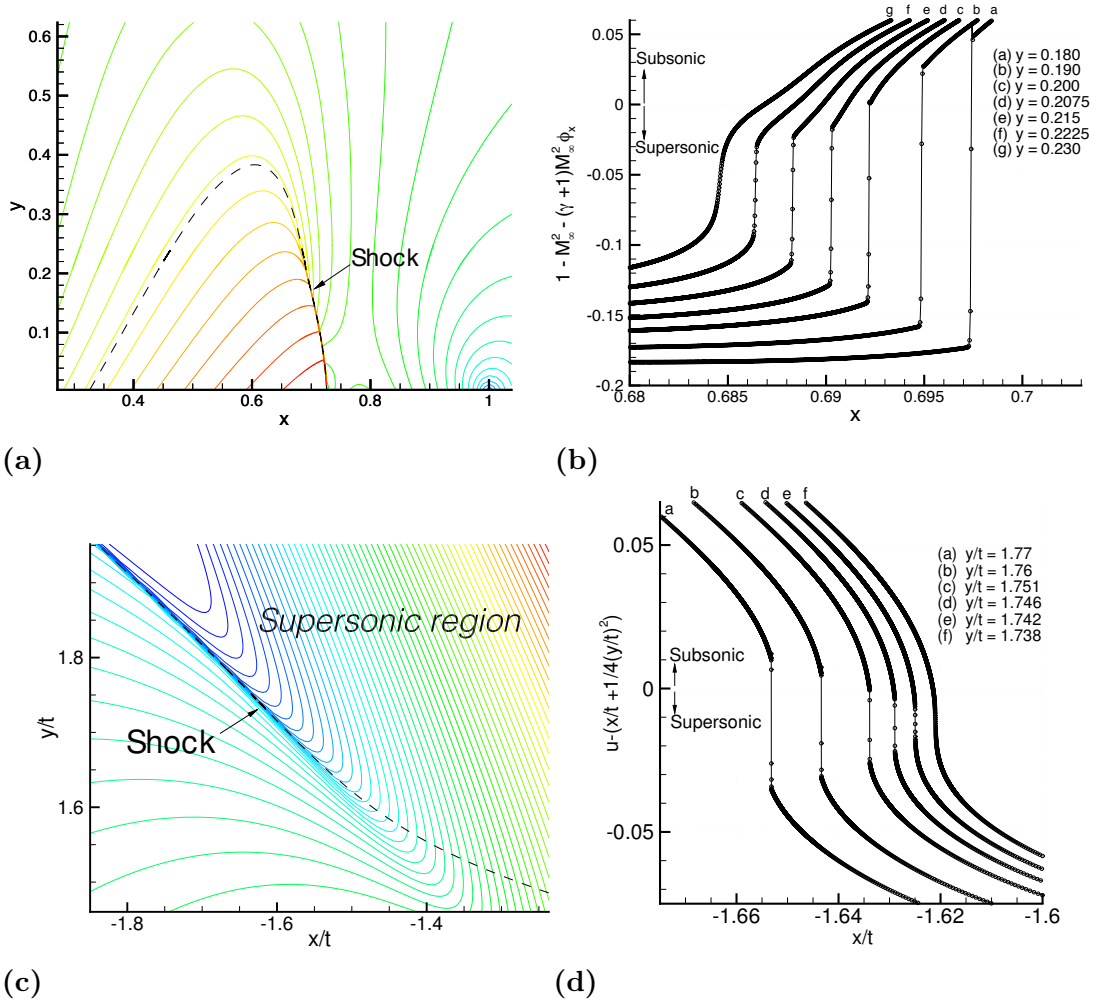

Figure 5.1: Numerical solutions for two problems for shock formation, as obtained in [8]. The plot in (a) depicts a solution of the steady TSDE for transonic flow over an airfoil at $M_\infty = 0.8$. Shown are u-contours and the (dashed) sonic line; the u-contour spacing is 0.03. The plot in (b) shows cross sections of the sonic function taken across the shock near the formation point; these profiles show that the shock begins between $y = 0.230$ and $y = 0.2225$, in the supersonic region. The plot in (c) shows u-contours and the sonic (dashed) line depicting a solution of a self-similar problem for the UTSDE describing diverging rarefactions; the u-contour spacing is 0.0075. The plot in (d) shows cross sections of sonic function S near the apparent shock formation point, showing that the shock forms at $y/t \approx 1.738$ in the supersonic region. The locally refined grids in these two solutions have grid spacings of $\Delta x = \Delta y = 1 \times 10^{-5}$ in (a), and $\Delta(x/t) = \Delta(y/t) = 5 \times 10^{-6}$ in (c).

numerical solution of a self-similar problem for the UTSDE describing the interaction of diverging rarefactions. Shown in this plot are u-contours and the sonic line close to the region where a shock forms, and again, the shock appears to form on the sonic line. The plot in (d) shows cross sections of the sonic function S for the self-similar UTSDE taken across the shock near its formation point. The cross sections taken very close to the actual formation point located at $y/t \approx 1.738$ contain jumps in S from supersonic to supersonic values. This again indicates that the shock forms at a supersonic point, away from the sonic line. The contrast between the shock profile plots in Fig. 5.1(b,d), and the one in Fig. 4.3, is striking.

In obtaining the final, highly refined solution shown in Figs. 4.2(a) and the accompanying shock profile plots in Figs. 4.2(b)-4.3, we computed solutions on successively refined grids, interpolated those onto more refined grids, and continued the process until no further change was observed in the solution near the shock disappearance point. This suggests that the final solution shown is grid converged. In addition, the resolution of the most refined grid used in the computation in this paper is comparable to the resolution of the locally refined grids used in the computations for shock formation in [8] (these grid resolutions are given in the captions for Figs. 4.2 and 5.1). Hence, it appears unlikely that further mesh refinement in this problem will result in the shock disappearance point moving off the sonic line and into the supersonic region, but we cannot rule out such a possibility. We also believe it is unlikely that the use of different high order numerical methods, or methods with higher orders of accuracy, will change the conclusion of sonic shock disappearance. Further investigation, however, is required to determine this conclusively.

We found that the use of the "nonlinearized" matching data in (2.6) as a numerical boundary condition gave results that were significantly different, and better, than those obtained using the linearized matching data in (2.4). The two solutions depicted in Fig. 4.5(a–b), which were computed on identical grids and at identical parameter values, but using the two different boundary conditions, illustrate several of the differences. First, the nonlinearized matching data displaces the shock forward in relation to its location given by the linearized data, as illustrated (see (3.7)). We also found that the wavefronts (shock or expansion) exited the numerical boundaries smoothly when the noninearized data was used, but that sometimes there were reflections when the linearized data was used. This is illustrated in the plot in (a), which shows a reflected wave behind the expansion wavefront at the bottom boundary. In addition, there were differences in the values of (u, v) in the subsonic portion of the flowfields, as illustrated by the different contour colors in the two plots. This is due to the fact that the two boundary conditions yield different values of (u, v) on the numerical boundaries, and (2.3) is elliptic in this part of the numerical domain. We also found that solutions converged with no difficulty when the nonlinearized boundary condition was used. On the other hand, when (2.4) was used, solutions would sometimes fail to converge, or converge very slowly. All of these effects appear to be due to the fact that (2.6) provides more accurate far-field matching data than (2.4).

We found that computing solutions using sufficiently large values of α was numerically unstable. When α was less than approximately 0.45, we were able to compute solutions, and converge them to machine accuracy, using CFL numbers which were typ-

ically in the range $0.25 - 0.4$. (These stable values of CFL number are similar to values we have used in computations done on shock reflection and shock formation problems using the same underlying numerical method.) For larger values of α, however, no choice of CFL number, however small, gave a stable computation. This instability is not relevant for the original weak-shock diffraction problem, which corresponds to the limit $\alpha \to 0$. Nevertheless, the parameter α cannot be removed from the UTSDE problem by rescaling, and these numerical results raise the question (not addressed here) of whether bifurcations from the small-α solution occur as α increases, conceivably leading to the non-existence of solutions when α is sufficiently large.

6 Conclusion

We have presented numerical solutions of a problem describing a shock that propagates into a constant state and diffracts self-similarly into an expansion wave. Our solutions provide evidence that the shock disappears on the sonic line where the self-similar equations change type. This differs from solutions for shock formation in steady transonic flows and self-similar flows by the compression of characteristics reflected off the sonic line, in which the shock typically forms inside the supersonic region.

7 References

[1] M. Delanaye, P. Geuzaine, and J. A. Essers, *Development and application of quadratic reconstruction schemes for compressible flows on unstructured adaptive grids*, AIAA Paper 97-2120, (1997), pp. 250–260.

[2] K. G. Guderley, *The Theory of Transonic Flow*, Pergamon Press, Oxford, UK, Addison-Wesley, Reading, MA, 1962.

[3] M. Hafez, J. C. South, E. M. Murman, *Artificial compressibility method for numerical solution of transonic full potential equation*, AIAA J., 17 (1979), pp. 145–152.

[4] J. K. Hunter and A. M. Tesdall, *On the self-similar diffraction of a weak shock into an expansion wavefront*, SIAM J. Appl. Math., to appear.

[5] A. Jameson, *Iterative solutions of transonic flows over airfoils and wings, including flows at Mach 1*, Communications on Pure and Applied Mathematics, 27 (1974), pp. 283–309.

[6] E. M. Murman, Analysis of embedded shock waves calculated by relaxation methods, AIAA J., 12 (1974), pp. 626–633.

[7] V. Shankar, I. Hiroshi, J. Gorski, S. Osher, *A fast, time accurate unsteady full potential scheme*, AIAA Paper 85-1512, Proc. AIAA 7th Computational Fluid Dynamics Conference (1985), pp. 214–227.

[8] A. M. Tesdall, *High resolution solutions for the supersonic formation of shocks in transonic flow*, Journal of Hyperbolic Differential Equations, 8 (2011), pp. 485–506.

[9] A. M. Tesdall and J. K. Hunter, *Self-similar solutions for weak shock reflection*, SIAM J. Appl. Math., 63 (2002), pp. 42–61.